

## Modeling the inactivation kinetics of lactic acid bacteria in a spray dryer

Dongbiao Jin, Houjuan Mao, Jie Xiao, Huanhuan Zhang, Meng Wai Woo, Xiao Dong Chen & Nan Fu

To cite this article: Dongbiao Jin, Houjuan Mao, Jie Xiao, Huanhuan Zhang, Meng Wai Woo, Xiao Dong Chen & Nan Fu (2023) Modeling the inactivation kinetics of lactic acid bacteria in a spray dryer, *Drying Technology*, 41:15, 2385-2404, DOI: [10.1080/07373937.2023.2245891](https://doi.org/10.1080/07373937.2023.2245891)

To link to this article: <https://doi.org/10.1080/07373937.2023.2245891>



View supplementary material [↗](#)



Published online: 17 Aug 2023.



Submit your article to this journal [↗](#)



Article views: 65



View related articles [↗](#)



View Crossmark data [↗](#)



## Modeling the inactivation kinetics of lactic acid bacteria in a spray dryer

Dongbiao Jin<sup>a</sup>, Houjuan Mao<sup>a</sup>, Jie Xiao<sup>a</sup>, Huanhuan Zhang<sup>a</sup>, Meng Wai Woo<sup>b</sup>, Xiao Dong Chen<sup>a</sup>, and Nan Fu<sup>a</sup>

<sup>a</sup>Suzhou Key Laboratory of Green Chemical Engineering, School of Chemical and Environmental Engineering, College of Chemistry, Chemical Engineering and Materials Science, Soochow University, Suzhou, Jiangsu, China; <sup>b</sup>Department of Chemical and Materials Engineering, The University of Auckland, Auckland, New Zealand

### ABSTRACT

Changes in the viability of probiotic cells during spray drying were tracked, by developing an inactivation model of *Lactobacillus rhamnosus* GG (LGG) and coupling the model to the drying kinetics of spray drying using Computational Fluid Dynamics simulation. Six inactivation models in the Arrhenius-equation form were developed using single droplet drying experiments with average drying rates of 0.011–0.044 kg/kg/s; all gave reliable goodness-of-fit. In simulating spray drying process, the predicted moisture content of LGG-containing particles well followed experimental trends. However, only inactivation model 6, which incorporated droplet temperature, moisture content, rate of temperature change, and drying rate, accurately predicted the survival of LGG. Models 1–5 that incorporated fewer kinetics parameters with higher activation energy values underestimated the degree of inactivation. The findings highlighted the crucial effects of the rates of temperature and moisture content change on the inactivation of probiotics during rapid drying with average drying rates of 0.31–0.81 kg/kg/s.

### ARTICLE HISTORY

Received 25 May 2023  
Revised 21 July 2023  
Accepted 4 August 2023

### KEYWORDS

Active dry probiotics; CFD; drying kinetics; inactivation model; probiotics powder; spray drying


## Introduction

Lactic acid bacteria (LAB) are Gram-positive, oxygen-tolerant bacteria widely applied in food, pharmaceutical, and agricultural industries as starter cultures, probiotics, and biopreservatives.<sup>[1]</sup> In most applications, the viability of LAB is a key criterion for fermenting dairy substances, acting beneficially on the host's health, and modifying the environment. Converting the living culture grown in a liquid medium to an active powder form can extend the shelf life of LAB products remarkably, and is advantageous to transportation and further dosage formulation.<sup>[2]</sup> Compared to the conventional freeze drying technique to produce active LAB powders, spray drying is cost-effective, rapid in powder production, and viable for large-scale production.<sup>[3]</sup> In spray drying, liquid feed that contains viable LAB cells and protectants is atomized into billions of micron-sized droplets, and then mixed with hot airflow for rapid conversion to dry particles in several to tens of seconds. With the rapid decrease in moisture content, the temperature of the droplets rises, which may lead

to severe dehydration and thermal stresses on LAB cells in the droplets.<sup>[4,5]</sup> Previous studies have proposed various protective approaches to improve the survival of LAB after spray drying, covering the entire powder production process from the cultivation of LAB to the drying and storage processes.<sup>[6–8]</sup> However, relatively little is known about the deactivation of LAB during the droplet-to-particle transition inside the spray dryer, where significant loss of bacterial viability up to several orders of magnitude may occur with severe cellular injuries.

Since it is relatively difficult to take samples of individual flying droplets inside a spray dryer, experimental and numerical approaches have been developed to investigate the coupled physicochemical transitions during spray drying. With the single droplet drying experiments, the drying kinetics of an isolated droplet can be accurately measured under conditions analogous to spray drying, contributing fundamental data needed in modeling a spray drying process.<sup>[9,10]</sup> Several studies have employed the technique to obtain the inactivation curves of LAB for various drying conditions and

**CONTACT** Jie Xiao ✉ [jie.xiao@suda.edu.cn](mailto:jie.xiao@suda.edu.cn); Nan Fu ✉ [nan.fu@suda.edu.cn](mailto:nan.fu@suda.edu.cn) Suzhou Key Laboratory of Green Chemical Engineering, School of Chemical and Environmental Engineering, College of Chemistry, Chemical Engineering and Materials Science, Soochow University, 199 Ren-Ai Rd., Suzhou Industrial Park, Suzhou, Jiangsu 215123, China

 Supplemental data for this article can be accessed online at <https://doi.org/10.1080/07373937.2023.2245891>.

© 2023 Taylor & Francis Group, LLC

protectants.<sup>[5,10–12]</sup> Numerical simulation approaches such as Computational Fluid Dynamics (CFD) have also been developed to track the drying processes of individual droplets inside a spray dryer. Through three-dimensional simulation, velocity and temperature fields in the dryer and the corresponding changing processes of the physicochemical properties of individual droplets can be described. The numerical simulation of spray drying has been carried out to investigate a number of problems that affect the quality of spray-dried particles, including drying kinetics, wall deposition, agglomeration, swirling flow, and so forth.<sup>[13–16]</sup>

The simulation of the inactivation of LAB during spray drying should be achieved by correlating the inactivation to drying kinetics experienced by bacterial cells in atomized droplets. By coupling a reliable inactivation model of LAB to the drying process of atomized droplets using CFD, it would be feasible to describe the changes in LAB viability during droplet drying. In the thermal processing of food, the rate of change of a quality attribute ( $C$ ) at different processing temperatures is conventionally described by the Arrhenius equation:<sup>[17]</sup>

$$-\frac{dC}{dt} = kC \quad (1)$$

$$k = k_0 \exp\left(-\frac{E}{RT}\right) \quad (2)$$

where  $t$  is the time of exposure, herein drying time (s),  $T$  refers to the temperature during constant-temperature processing (K) and  $k$  is the corresponding rate constant of quality change,  $E$  is the activation energy needed for the change to occur, and  $k_0$  is a pre-exponential factor. Fu et al. employed Equation (2) to describe the inactivation process of *Lactococcus lactis* ssp. *cremoris* during single droplet drying, taking the inactivation rate  $k_d$  as the rate change of the survival of bacteria ( $N/N_0$ , with  $N$  being the viable cell count of bacteria, cfu/mL) as drying progressed.<sup>[10]</sup> With an  $E_d$  of 105.50 kJ/mol and  $k_0$  of  $2.84 \times 10^{14}$ , Equation (2) well described the inactivation profiles of *L. cremoris* at six single droplet drying conditions, that is, feed solid contents of 10 and 20 wt% and drying temperatures of 70, 90, and 110 °C.<sup>[10]</sup>

In spray drying, the majority of water in atomized droplets can be removed in several to tens of seconds, which is much shorter than the drying time of around 2–10 min in a single droplet drying process. The associated high rates of temperature change and water removal may cause a higher loss of bacterial viability than a slow application of the stresses.<sup>[18,19]</sup> Such a characteristic might be linked to the nature of living

microorganisms, which show significant differences from bioactive chemicals such as proteins and vitamins toward stresses.<sup>[8]</sup> For instance, bacterial cells could experience multiple cellular injuries during dehydration,<sup>[20,21]</sup> and may repair the injuries and continue multiplying under suitable conditions. Chen and Patel proposed a series of modified Arrhenius equations to account for the effects of the rate of temperature change ( $dT/dt$ ) and drying rate ( $-dX/dt$ ) on the inactivation of bacteria (Table 1), where  $X$  is moisture content on a dry basis (kg/kg).<sup>[22]</sup> Huang et al. applied the equations to describe the inactivation of yeast during infrared drying.<sup>[23]</sup> It was found that the model that incorporated  $T$ ,  $dT/dt$ , and  $-dX/dt$  gave a more accurate prediction of the experimental survival curve than the simple Arrhenius equation that included  $T$  as the only parameter.<sup>[23]</sup> However, it has remained unclear to what extent the drying kinetics parameters affected the inactivation of bacteria and how the effects vary with different drying conditions, which are crucial to developing a suitable inactivation model for various drying applications. To date, there is yet an inactivation model that can capture the changes in the viability of bacterial cells during spray drying.

The objective of the present study is to describe the inactivation process of LAB inside a spray dryer numerically, by developing an inactivation model that takes into account the effects of drying kinetics parameters and coupling the model to the drying kinetics of spray drying using CFD. Six inactivation models of a model probiotic strain, *Lactobacillus rhamnosus* GG, were established based on reported single droplet drying data.<sup>[5,24]</sup> The inactivation models were coupled to the dryer scale Multiphysics drying kinetics model of a microfluidic jet spray dryer on the FLUENT platform. The spray dryer generated monodisperse atomized droplets for dehydration under well-controlled drying conditions, so the produced particles were uniform in size, morphology, and properties.<sup>[25]</sup> The simulation results were compared to the experimental results of the spray drying of *L. rhamnosus* GG to identify the appropriate inactivation model. Changes in the viability of *L. rhamnosus* GG inside the spray dryer were unveiled, and the effects of drying kinetics parameters on the viability of the bacteria in spray drying, a typical rapid drying process, were discussed.

## Modeling and analysis methods

### Problem statement and system description

A schematic of the spray dryer studied in the present study is shown in Figure 1a. Its working principles

**Table 1.** Arrhenius equation and modified Arrhenius equations describing the inactivation of lactic acid bacteria during convective drying.

Model No.	Equation*	Variables
1	$\frac{dC}{dt} = -k_0 C \exp\left(-\frac{E_d}{RT}\right)$	$T$
2	$\frac{dC}{dt} = -k_0 C \exp\left(aX - \frac{E_d}{RT}\right)$	$T, X$
3	$\frac{dC}{dt} = -k_0 C \left(1 + c \cdot \left  -\frac{dX}{dt} \right  \right) \exp\left(-\frac{E_d}{RT}\right)$	$T, -\frac{dX}{dt}$
4	$\frac{dC}{dt} = -k_0 C \left(1 + c \cdot \left  -\frac{dX}{dt} \right  \right) \exp\left(aX - \frac{E_d}{RT}\right)$	$T, X, -\frac{dX}{dt}$
5	$\frac{dC}{dt} = -k_0 C \left(1 + b \cdot \left  \frac{dT}{dt} \right  \right) \exp\left(aX - \frac{E_d}{RT}\right)$	$T, X, \frac{dT}{dt}$
6	$\frac{dC}{dt} = -k_0 C \left(1 + b \cdot \left  \frac{dT}{dt} \right  \right) \left(1 + c \cdot \left  -\frac{dX}{dt} \right  \right) \exp\left(aX - \frac{E_d}{RT}\right)$	$T, X, \frac{dT}{dt}, -\frac{dX}{dt}$

\*C refers to the survival of bacteria ( $N/N_0$ ), and the subscript  $d$  represents deactivation.

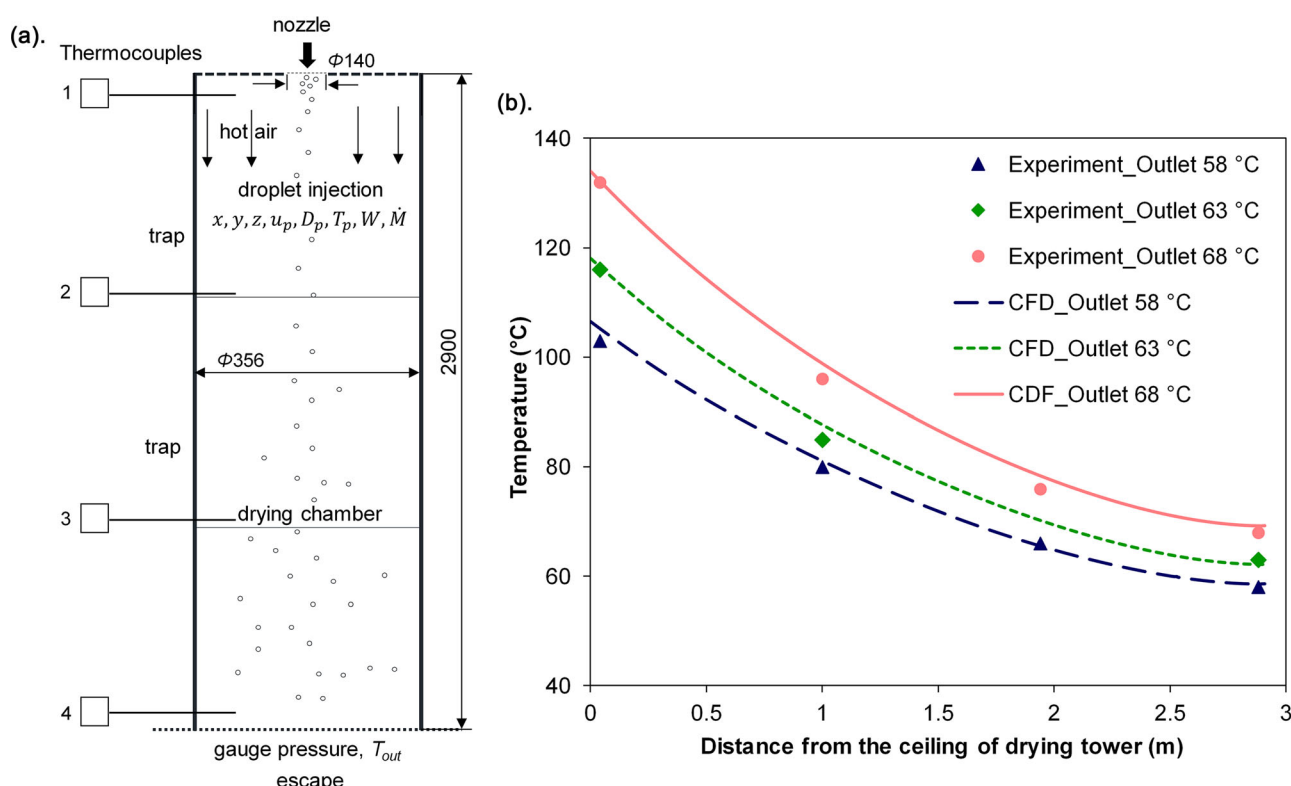


**Figure 1.** (a) The schematic of microfluidic jet spray dryer used to produce *L. rhamnosus* GG powder in the current study (not to scale in mm); (b) comparison of the temperature profile of flow field in the CFD simulation to the experimental values measured by four thermocouples placed in the spray dryer.

and experimental procedures have been described in detail in previous studies.<sup>[25]</sup> To produce active *L. rhamnosus* GG powder, monodisperse droplets containing viable *L. rhamnosus* GG cells with reconstituted skim milk (RSM) as protectant are injected into the drying chamber from the nozzle. The hot air flows co-currently into the tower from tiny holes that are evenly distributed on the ceiling of the drying tower. Dried particles can be directly collected at the outlet of the cylindrical chamber. In typical experimental studies, the remaining viability of *L. rhamnosus* GG in spray-dried powder is analyzed, and compared to the value in the feed to calculate the survival of the

bacteria after spray drying.<sup>[26]</sup> Clearly, survival at the outlet of the dryer is the cumulative result of the inactivation process of the bacteria inside the dryer, during which viable cells are carried in atomized droplets and experience changes in the droplet environment as droplets are transformed into particles. Such changes in bacterial viability, also known as inactivation history, are complicated to track experimentally. The structure of the spray dryer does not allow frequent and convenient sampling of droplets flying in the drying chamber. CFD simulation offers a quantitative approach to unveil the complex physico-chemical transitions inside a spray dryer.

### Governing equations

The drying air flow is modeled with 3D Navier-Stokes conservation equations integrated with RNG k- $\epsilon$  turbulent model to capture the slightly turbulent flow in the chamber.<sup>[27]</sup> The interactive heat and mass transfer between air (bulk fluid) and atomized droplets (discrete particles) is described with the discrete phase model (DPM), and the evaporation process of individual droplets is modeled with the Reaction Engineering Approach (REA). Most importantly, in this work, to describe changes in the viability of bacteria in the droplets, the key is the development of a model that is capable of correlating bacterial viability ( $N$ ) to the kinetic parameters (i.e., temperature, moisture content, and their changing rates) of the droplets being dried. The governing equations for the droplet model are listed below.

### Droplet trajectory determination

During drying, droplets and the flow field affect each other interactively. The trajectories of the droplets are mainly determined by the initial speed and the drag force of the fluid. The following equations for spherical droplets are used:

$$\begin{cases} \frac{d\vec{u}_p}{dt} = \frac{(\vec{u} - \vec{u}_p)}{\tau_r} + \frac{\vec{g}(\rho_p - \rho)}{\rho_p} + \frac{\vec{F}}{m_p} \\ \tau_r = \frac{\rho_p D_p^2}{18\mu} \frac{24}{C_d Re} \\ Re = \frac{\rho D_p |\vec{u} - \vec{u}_p|}{\mu} \end{cases} \quad (3)$$

where  $\vec{u}_p$  is the velocity of droplets (m/s),  $\vec{u}$  is the velocity of hot air (m/s),  $D_p$  is the diameter of a droplet, and  $C_d$  is the drag coefficient calculated using an empirical correlation between  $C_d$  and  $Re$ .<sup>[28]</sup>

### Droplet shrinkage model

A falling droplet is assumed spherical and shrinks uniformly as water is removed from the droplet. The correlation between droplet diameter  $D_p$  and its moisture content  $X$  (kg/kg) is described by the linear shrinkage model as reported by Line and Chen:<sup>[29]</sup>

$$\frac{D_p}{D_{p,0}} = \alpha + (1 - \alpha) \frac{X}{X_0} \quad (4)$$

where  $\alpha$  is taken as 0.51, 0.59, and 0.69 for 10 wt%, 20, and 30 wt% RSM droplets, respectively.

The conservation of heat during spray drying and the heat balance between droplets and gas involving moisture evaporation are calculated using the following equations:

$$\begin{cases} m_p c_{p,p} \frac{dT_p}{dt} - \Delta H_l \frac{dm_p}{dt} = A_p h (T_b - T_p) \\ \frac{\partial(\rho E)}{\partial t} + \nabla \cdot [\vec{u}(\rho E + p)] \\ = \nabla \cdot [k_{eff} \nabla T - \sum_j h_j \vec{J}_j + (\vec{\tau}_{eff} \cdot \vec{u})] - n \frac{dm_p}{dt} \Delta H_l \end{cases} \quad (5)$$

where  $T_p$  and  $T_b$  are droplet temperature and bulk air temperature (K), respectively,  $h$  is the heat transfer coefficient (W/(m<sup>2</sup>·K)), and  $\Delta H_l$  is the specific enthalpy of water evaporation (J/kg). The second expression of Equation (5) is the energy conservation equation solved in FLUENT, where  $k_{eff}$  is the effective thermal conductivity (W/(m·K)), and  $\vec{J}_j$  is the diffusion flux of species  $j$  (Kg/(m<sup>2</sup>·s)). The last term on the right of the second expression refers to energy transfer due to water evaporation.

### Droplet evaporation model

Evaporation causes the transfer of moisture from the droplets to the gas phase under the driving force of the difference in vapor density between the droplet surface and bulk gas. The rate of drying ( $-dm_p/dt$ ) can be mathematically denoted as:

$$\frac{dm_p}{dt} = m_s \frac{dX}{dt} = -h_m A_p (\rho_{v,sur} - \rho_{v,b}) \quad (6)$$

$$\frac{dm_b}{dt} = h_m A_p (\rho_{v,sur} - \rho_{v,b}) \quad (7)$$

where  $m_s$  is the mass of solids in the droplets (kg),  $h_m$  represents the mass transfer coefficient (m/s), and  $\rho_{v,sur}$  and  $\rho_{v,b}$  are water vapor density at the droplet surface and the flow field (kg/m<sup>3</sup>), respectively. Since  $\rho_{v,sur}$  is in a transient state during drying, a fractional coefficient  $\psi$  is introduced to correlate it with the saturated vapor density at the droplet surface ( $\rho_{v,sat}$ ) according to the REA model:<sup>[30]</sup>

$$\rho_{v,sur} = \psi \rho_{v,sat}(T_{sur}) \quad (8)$$

where  $T_{sur}$  is the surface temperature of the droplet (K). For micron-sized droplets like atomized droplets during spray drying, the temperature gradient in the radial direction may be neglected,<sup>[30]</sup> and  $T_{sur}$  is approximated as the average temperature of the droplet  $T_p$  in the present study.

In describing droplet drying kinetics, the lumped REA (L-REA) model considers the evaporation of water as an activation-energy-based process that needs to overcome an energy barrier to occur. The fractional coefficient  $\psi$  can be correlated with the apparent activation energy of evaporation,  $\Delta E_v$ , using an Arrhenius-type equation:



$$\psi = \exp \left( -\frac{\Delta E_v}{RT_p} \right) \quad (9)$$

Extensive studies have demonstrated that changes in the activation energy  $\Delta E_v$  during the drying of a given material can be correlated with the changes in its moisture content using a generalized equation for varying drying conditions, as far as the initial solid content of the material is the same:<sup>[30]</sup>

$$\frac{\Delta E_v}{\Delta E_{v,b}} = f(X - X_e) \quad (10)$$

where  $\Delta E_{v,b}$  is the maximum activation energy when the moisture content of the material reaches equilibrium with the bulk gas at a specific drying condition, and  $X_e$  is the corresponding equilibrium moisture content.  $X_e$  can be calculated with the GAB equation in the following form:

$$\begin{cases} X_e = \frac{CKm_0a_w}{(1 - Ka_w)(1 - Ka_w + CKa_w)} \\ C = C_0 \exp \left( \frac{\Delta H_1}{RT} \right) \\ K = K_0 \exp \left( \frac{\Delta H_2}{RT} \right) \end{cases} \quad (11)$$

where  $a_w$  is the water activity of the bulk gas,  $m_0$  is the monolayer moisture content, and parameters  $C$  and  $K$  are functions of gas temperature. In the present study, RSM is used as protectant, and the mass of LAB cells is considered negligible compared to the mass of milk solids, so the parameters of RSM are used, that is,  $m_0$ ,  $C_0$ ,  $\Delta H_1$ ,  $K_0$ ,  $\Delta H_2$  values of 0.06156 kg/kg, 0.001645, 24831 J/mol, 5.710, and -5118 J/mol, respectively.<sup>[30]</sup>

For drying a given material, Equation (10) is a characteristic fingerprint model established with the REA concept. The specific form of the equation can be determined through a minimum number of experiments, and then the established model can be used to describe drying kinetics under other conditions. The model used for the drying of RSM droplets in the present study is reported by Chen and Lin:<sup>[30]</sup>

$$\frac{\Delta E_v}{\Delta E_{v,b}} = 0.998 \exp [-1.405(X - X_e)^{0.930}] \quad (12)$$

### Inactivation model of viable bacteria

Models 1–6 in Table 1 provide several possibilities for developing an inactivation model in the Arrhenius-equation form. The corresponding model parameters,  $a$ ,  $b$ , and  $c$ , should be determined before the inactivation model can be coupled with a CFD model of spray

drying. In this study, the inactivation data of *L. rhamnosus* GG reported in previous single droplet drying studies<sup>[5,24]</sup> are used to fit Models 1–6 to determine the parameters for each model. Specifically, single droplet drying experiments offer dynamic data on the survival of bacteria ( $N/N_0$ ) throughout the complete drying process. Fitting the models to the experimental data is achieved by solving the optimization problem with  $\min_{\theta} \left[ \sum (N/N_{0calc,i} - N/N_{0experiment,i})^2 \right]$  as the target function, where  $i$  is the index of sampling time instant and  $\theta$  is the set containing model parameters,  $a$ ,  $b$ , and  $c$ . The experimental data used to develop the parameters for each model are from four single droplet drying conditions (Trial 1, 2, 4, and 5 in Table 2), with varying initial droplet size (1 or 2  $\mu$ L), initial solids content (10 or 20 wt%), drying air temperature (70 or 90 °C), and airflow velocity (0.45, 0.75, and 1 m/s). The obtained  $a$ ,  $b$ , and  $c$  values are employed to predict the survival of *L. rhamnosus* GG for a separate single droplet drying condition (Trial 3 in Table 2), to examine the predictive performance of each equation.

The resulting six inactivation models are coupled to the CFD model of the spray drying of *L. rhamnosus* GG through user defined functions (UDFs), respectively. The survival of the bacteria at the dryer outlet predicted by each inactivation model is compared to the experimental survival in spray-dried *L. rhamnosus* GG powders, to determine the model that gives the most accurate description of the inactivation of the bacteria during spray drying.

### Boundary and initial conditions

Table 3 summarizes the boundary conditions of airflow used in the calculation of the main drying chamber. Following the conditions used in the spray drying experiments, three inlet temperatures of 106, 118, and 134 °C are used to control the outlet temperature of the drying chamber at 58, 63, and 68 °C, respectively. The heat loss of the spray dryer is considered by incorporating the convective heat transfer coefficient of the dryer wall, as shown in Table 3. Table 4 summarizes the initial conditions of the discrete phase and the corresponding experimental results obtained with the microfluidic jet spray dryer. The injected droplets are considered monodisperse, with an initial droplet size of 155  $\mu$ m.<sup>[25]</sup> At the outlet temperature of 58 °C, skim milk at three initial solid contents (10, 20, and 30 wt%) are used as the protectant of *L. rhamnosus* GG, respectively. At 63 °C, 20 wt% skim milk is used.

**Table 2.** Experimental conditions used in the single droplet drying of *L. rhamnosus* GG, with reconstituted skim milk (RSM) as protectant.

Trial No.	Airflow conditions		Droplet conditions		Note
	Temperature (°C)	Velocity (m/s)	Initial solid content (wt%)	Initial droplet size (μL)	
1	70	0.45	20	1	Development of model parameters
2	70	1	20	1	
3	70	0.45	20	2	Comparison with model prediction
4	70	1	20	2	
5	90	0.75	10	2	

**Table 3.** Boundary conditions of the spray drying chamber in the CFD simulation.

Outer annulus inlet of air:	
Direction	Normal
Volumetric flow rate (L·min <sup>-1</sup> )	250
Temperature (°C)	106, 118, 134*
Water vapor mass fraction (kg H <sub>2</sub> O/kg air)	0.01
Central inlet of disperse air:	
Direction	Normal
Volumetric flow rate (L·min <sup>-1</sup> )	8
Temperature (°C)	35
Water vapor mass fraction (kg H <sub>2</sub> O/kg air)	0.0001
Outlet:	
Gauge pressure (Pa)	0
Backflow temperature (°C)	25
Wall:	
Convective heat transfer coefficient (W · m <sup>-2</sup> · K <sup>-1</sup> )	1.8, 1.8, 1.8
Free stream temperature (°C)	25

\*The setting of inlet temperature was to control the outlet temperature of drying chamber at 58, 63, and 68 °C, respectively, in accordance with the experiment conditions used to produce *L. rhamnosus* GG powders.

## Results and discussion

### Establishment of a kinetic model for the inactivation of *L. rhamnosus* GG using the single droplet drying experiment

Experimental data from four single droplet drying experiments (Trial 1, 2, 4, and 5 in Table 2) were used to obtain parameters *a*, *b*, and *c* in Models 1–6 (Table 1), and the predictive performance of the resulting six models on the inactivation of *L. rhamnosus* GG during convective droplet drying was evaluated by comparing to Trial 3. To gain a better understanding of the different forms of the kinetic model, the inactivation processes of *L. cremoris* under eight conditions were also modeled with Models 1–6, in which experimental data from six conditions were used to obtain parameters *a*, *b*, and *c* for each model, and the other two experiments were used to evaluate the predictive performance (Table S1, supplementary material). The optimal parameters for each model to describe the inactivation of *L. rhamnosus* GG and *L. cremoris* are shown in Table 5 and Table S2 (supplementary material), respectively.

In describing the inactivation of *L. rhamnosus* GG, the trends given by all six models well followed the

experimental data as shown in Figure 2, with *R*<sup>2</sup> larger than 0.90 (Table 5). On a normal scale between 0 and 100%, the six curves were close to each other at each tested condition (Figure 2a–d), whereas divergence was observed at a later drying stage when the data were plotted on a logarithmic scale (Figure 2A–D). In Figure 2B and D, Model 1 which only considered the effect of *T* showed the lowest similarity to experimental data, while in Figure 2A and C it was Model 2, which considered the effects of both *X* and *T*. Models 3–6 that took the effects of the rates of change into account showed similar goodness-of-fit, giving higher *R*<sup>2</sup> (larger than 0.92) than Models 1 and 2. To verify the reliability of these equations, the survival data of *L. rhamnosus* GG during Trial 3 were predicted with each model. The resulting six curves nearly overlapped each other (Figure 3).

It is worthwhile to note that the incorporation of an increasing number of kinetic parameters appeared to be associated with a perceptible decrease in the activation energy for the inactivation of LAB (*E<sub>a</sub>* in Table 5). The highest *E<sub>a</sub>* of 124,000 J/mol in deactivating *L. rhamnosus* GG was given by Model 1, whereas the lowest *E<sub>a</sub>* of 80,014 J/mol was achieved with Model 4 which involved *T*, *X*, and  $-dX/dt$ . Model 6 which considered the effect of four parameters (*T*, *X*,  $dT/dt$ , and  $-dX/dt$ ) showed the second lowest *E<sub>a</sub>* of 93,711 J/mol. A similar trend was observed in modeling the inactivation of *L. cremoris* during convective droplet drying (Table S2, supplementary material). With the increase in the number of kinetic parameters, *E<sub>a</sub>* gradually decreased from 117,500 J/mol in Model 1 to 69,634 J/mol in Model 6. The low activation energy value may indicate that the inactivation reaction could occur at a faster rate by overcoming a relatively low energy barrier. Moreover, the reaction with a low activation energy value is less sensitive to the change of temperature than that with a high value. By contrast, the inactivation model that incorporated fewer kinetic parameters might overestimate the activation energy, so the predicted degree of inactivation is likely lower than that predicted by a model with lower activation energy under the same reaction condition.

**Table 4.** Initial conditions of skim milk droplets containing *L. rhamnosus* GG for injection to the spray drying chamber in the CFD simulation, and the experimental survival of the bacteria and the moisture content of powders after spray drying under different conditions.

Parameters of droplets entering the spray drying chamber:	
Initial droplet size ( $\mu\text{m}$ )	155
Initial droplet temperature ( $^{\circ}\text{C}$ )	25
Initial velocity ( $\text{m} \cdot \text{s}^{-1}$ )	3.7
Mass flow rate ( $\text{kg} \cdot \text{s}^{-1}$ )	$2.2 \times 10^{-5}$
The density of skim milk solids ( $\text{kg} \cdot \text{m}^{-3}$ )	1530
The specific heat capacity of skim milk solids ( $\text{J} \cdot \text{kg}^{-1} \cdot \text{K}^{-1}$ )	1784
Experimental results for drying processes with an outlet temperature of $58^{\circ}\text{C}$	
Initial solid content (wt%)	10, 20, 30
Moisture content of spray dried powder (kg/kg)	$0.1082 \pm 0.0674$ , $0.1054 \pm 0.0117$ , $0.0854 \pm 0.0144$
Survival of LGG in the powder (%)	$16.67 \pm 11.67$ , $27.53 \pm 9.91$ , $33.94 \pm 17.97$
Experimental results for drying process with an outlet temperature of $63^{\circ}\text{C}$	
Initial solid content (wt%)	20
Moisture content of spray dried powder (kg/kg)	$0.0944 \pm 0.0186$
Survival of LGG in the powder (%)	$19.77 \pm 3.12$

**Table 5.** Optimal parameters for Models 1–6 to describe the inactivation of *L. rhamnosus* GG during convective droplet drying.

Model No.	Model parameters					Fitting performance*			Predictive performance*	
	$k_0$	$E_d$ ( $\text{J} \cdot \text{mol}^{-1}$ )	a	b	c	RMSE	$R^2$	AIC <sup>†</sup>	RMSE	$R^2$
1	$1.41 \times 10^{17}$	124000				0.1177	0.9178	−181.27	0.0797	0.9111
2	$3.57 \times 10^{14}$	105443	−1.43			0.1235	0.9095	−178.21	0.1171	0.8238
3	$5.18 \times 10^{16}$	121642			35.94	0.1110	0.9253	−188.50	0.1004	0.8597
4	$6.67 \times 10^{10}$	80014	−5.27		357.72	0.1126	0.9231	−185.14	0.0755	0.9192
5	$2.35 \times 10^{15}$	110510	−2.83	4.41		0.1140	0.9215	−184.78	0.0437	0.9406
6	$7.61 \times 10^{12}$	93711	−3.66	1.29	95.49	0.1105	0.9261	−183.45	0.0874	0.8994

\*Fitting performance refers to the comparison between model description and the experimental results of single droplet drying experiments No. 1, 2, 4, and 5 in Table 2. After the model parameters were determined with the four experiments, the prediction performance of each model was examined by comparing the model description and experimental results of single droplet drying experiment No. 3.

†AIC: Akaike information criterion.

In describing the inactivation of *L. cremoris* (Table S2, supplementary material), Model 5, which considered the effect of  $T$ ,  $X$ , and  $dT/dt$ , showed the worst description both in fitting the data from six experiments and in predicting the data from two separate experiments ( $R^2$  of 0.9133 and 0.8755, respectively). Compared to the description results of *L. rhamnosus* GG, the trends given by the six models on the inactivation of *L. cremoris* showed considerable discrepancy at each drying condition, for example, in Fig. S1B, S1E, S1F, S2A, and S2B (supplementary material).

The goodness-of-fit of each model in describing the inactivation processes of *L. rhamnosus* GG and *L. cremoris* was analyzed with the Akaike information criterion (AIC), as shown in Table 5 and Table S2 (supplementary material). For the inactivation of *L. rhamnosus* GG (Table 5), the incorporation of  $-dX/dt$ , which was a rate parameter, in Model 3 led to a perceptibly lowered AIC value (−188.50) compared to Models 1 and 2 which only considered the effects of  $T$  and  $X$  (−181.27 and −178.21, respectively), indicating a better fit. The incorporation of more drying kinetics

parameters in Models 4, 5, and 6 slightly increased the AIC value by 3–5. In general, the AIC values of the six models were in a similar range between −188.50 and −178.21, although the number of model parameters varied from 2 to 5 (Table 5). For the inactivation of *L. cremoris*, the lowest AIC values were observed with Models 1 and 2 (−382.45 and −382.46, respectively; Table S2, supplementary material). With the increase in the number of drying kinetics parameters, the AIC values gradually increased, indicating the penalty of AIC on the number of variables. Models 1–4 and 6 showed AIC values in a similar range between −382.46 and −360.58, whereas Model 5 gave the highest AIC of −319.64, indicating the worst fitting in describing the inactivation processes of *L. cremoris*.

Two criteria may be helpful in developing a suitable model to describe the inactivation of microorganisms. First, the parameters in the model should be interpretable with clear biological or physical meanings, and second, it should be capable of describing multiple inactivation processes under varying conditions using one set of parameters.<sup>[31]</sup> Apart from the



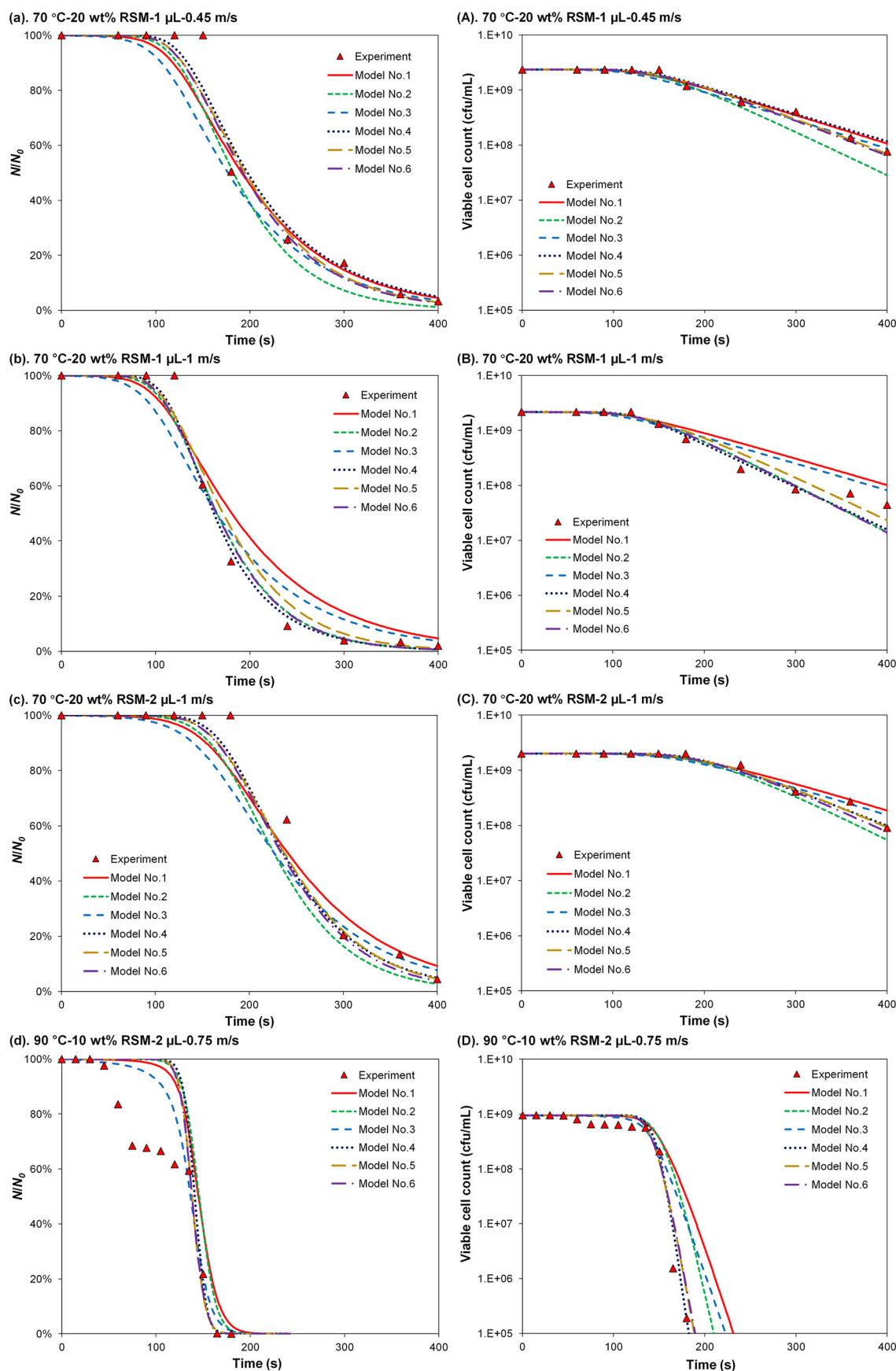


**Figure 2.** The description of the inactivation process of *L. rhamnosus* GG during four single droplet drying processes, by Models 1–6 incorporating optimal parameters in Table 5. (a–d) The survival of *L. rhamnosus* GG plotted on a normal scale; (A–D) the viable cell count of the bacteria plotted on a logarithmic scale. (a, A) Trial 1, (b, B) Trial 2, (c, C) Trial 4, and (d, D) Trial 5 in Table 2.

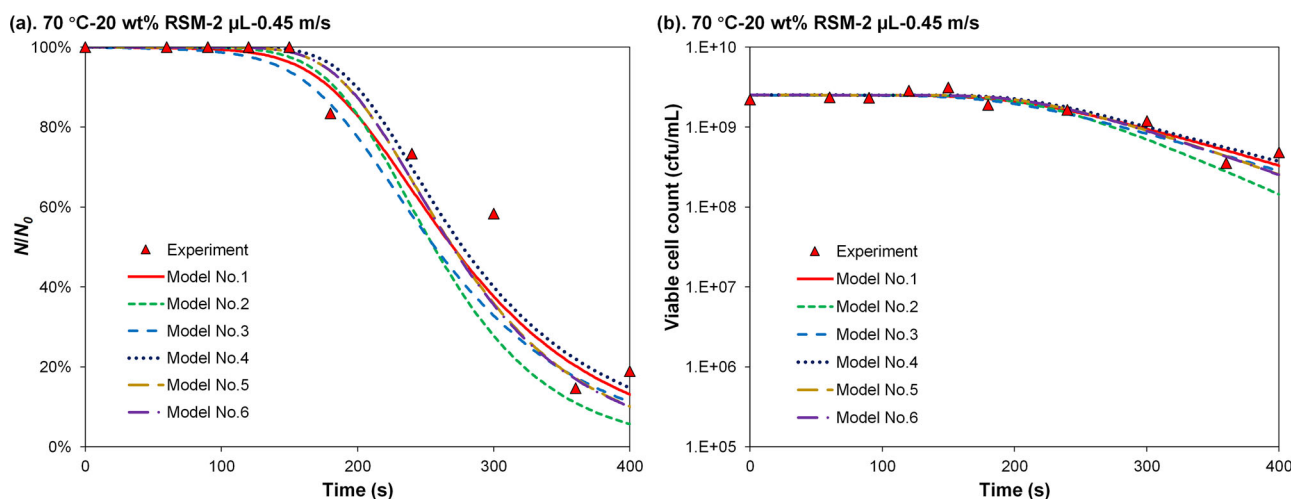


**Figure 3.** The validation of optimal parameters for each inactivation model, by comparing model prediction to the results of single droplet drying experiment No. 3 in Table 2. (a) The survival of *L. rhamnosus* GG plotted on a normal scale; (b) the viable cell count of the bacteria plotted on a logarithmic scale.

first-order kinetics model coupled with the activation energy theory used in the present study, the Weibull distribution model is another widely utilized inactivation model.<sup>[32]</sup> The Weibull model considers the inactivation of bacterial populations as the cumulative result of the distribution of lethal events, namely the inactivation of individual bacterial cells with varying stress resistance in the population. The model with an empirical nature has been successfully applied in describing a variety of inactivation processes during both thermal and nonthermal processes.<sup>[33,34]</sup> Furthermore, when the heat treatment is non-isothermal, the temperature history experienced by the bacteria can be correlated to model parameters to improve the accuracy of the description.<sup>[35]</sup> Nonetheless, during a dynamic drying process, bacterial cells experience dramatic changes in both environmental temperature and moisture content. The Arrhenius-type equations in Table 1 show high flexibility in incorporating kinetic parameters including the rates of change.

In a previous study, the survival of the spores of *Bacillus thuringiensis* after spray drying was correlated to the inlet and outlet temperatures of the spray dryer, respectively, using the Arrhenius equation.<sup>[36]</sup> Since the size and geometrical structure of spray dryer vary considerably from dryer to dryer, the survival of LAB could show remarkable differences when different dryers are used, even with the same inlet and outlet temperatures. In the present study, the droplet temperature is used to accurately capture the effect of temperature history experienced by LAB cells during convective droplet drying, and the histories of other kinetic parameters have also been taken into account.

The results in Figure 2, 3, S1, and S2 (supplementary material) validated the reasonableness of such modifications, namely, using droplet temperature instead of drying air temperature to develop the inactivation model. Since the goodness-of-fit and goodness-of-predication were similar regardless of the form of kinetic inactivation models, all six models for the inactivation of *L. rhamnosus* GG were coupled to the CFD model of spray drying process using parameters summarized in Table 5.

### Description of the inactivation process of *L. rhamnosus* GG during spray drying using kinetic inactivation models

The verification of CFD simulation to the experimental process of the microfluidic jet spray dryer was first carried out on the flow field without the injection of atomized droplets. Three outlet temperatures of 58, 63, and 68 °C were tested, achieved with inlet temperatures of 106, 118, and 134 °C, respectively (Figure 1b). The predicted temperatures at the location of thermocouple placement well matched the measured values under all three conditions. Then particles that simulated atomized droplets were injected into the flow field using the DPM model, with initial conditions shown in Table 4. The major constitute in the droplets was the protectant for LAB cells, namely RSM, with three initial solid contents of 10, 20, and 30 wt%, respectively. Four spray drying conditions were studied: three initial solid contents at an outlet temperature of 58 °C and the initial solid content of 20 wt% at 63 °C (Table 4).

After the state of injected droplets reached steady, their temperature, moisture content, diameter, and residence time profiles along the axis of the simulated spray dryer are shown in Figure 4. As the droplets traveled from the top inlet to the bottom outlet of the dryer, their temperature histories can be characterized with different drying stages (Figure 4a). In the spray drying of 10 wt% droplets at 58 °C, a pre-heating stage, a wet-bulb temperature range, a rapid heating stage, followed by a temperature-decreasing stage were observed.<sup>[24]</sup> With the increase in solid content, droplet temperature started to rise at the wet-bulb temperature range, and no wet-bulb stage was observed for the drying of 30 wt% RSM droplets at 58 °C. Increasing the outlet temperature from 58 to 63 °C resulted in an upward shift of the droplet temperature curve for the drying processes with 20 wt% RSM. The decrease in droplet temperature at the later drying stage was because droplet temperature reached the temperature of the flow field, and then decreased with the decline in the field temperature as the droplets approached the outlet. The decrease in the field temperature at the later drying stage mainly arose from the heat loss of the spray dryer. The droplet temperature profiles in general resembled those reported by Rogers et al.,<sup>[37]</sup> which were calculated using one-dimensional modeling for the spray drying of RSM. At 58 °C, RSM droplets with 10 wt% solids experienced the highest peak temperature, which was attributed to the lowest mass content as reflected in Figure 4c.<sup>[37]</sup>

The decrease in the moisture content of 10 wt% droplets became minimal at around 2.5 m from the top of the dryer, whereas that of 20 and 30 wt% droplets continued till the bottom outlet at the same outlet temperature (Figure 4b). Gong et al. took samples from the different heights of a spray dryer, and found that a significant loss of LAB viability (>90%) occurred when the droplet moisture content was lower than 0.31 kg/kg, associated with substantial damages on cellular membrane.<sup>[20]</sup> At 58 °C, the moisture content of atomized droplets reached lower than 0.31 kg/kg at around 1.8–1.9 m of the spray dryer, irrespective of the different initial moisture contents (Figure 4b). Nevertheless, the residence time of 30 wt% droplets was remarkably shorter than that of droplets with lower solid contents (Figure 4d). The shortened exposure time to a high-temperature environment may help retain the viability of LAB cells, making 30 wt% RSM potentially a more effective protectant than 10 and 20 wt% RSM. Increasing the outlet temperature from 58 to 63 °C led to perceptibly faster

moisture removal and correspondingly faster droplet shrinkage during spray drying (Figure 4b and c). The moisture content of droplets at the outlet of the simulated spray dryer was compared to the corresponding experimental value of spray dried particles in Figure 5. The experimental trends were correctly described, and the predicted values were similar to the experimental moisture content of LAB powders for all four conditions tested. The results verified the reliability of the simulated drying kinetics.

Figure 6 presented the inactivation profiles of *L. rhamnosus* GG, which were calculated by coupling the six inactivation models in Table 1 to the droplet drying kinetics in Figure 4 for each drying condition. The six models generated distinct inactivation profiles for each spray drying process, contrasting the similar trends given by different models in the single droplet drying experiments (Figures 1 and 2, Figure S1, S2, supplementary material). Significant loss of the viability of *L. rhamnosus* GG was only observed with Model 6, which not only considered the effects of  $T$  and  $X$ , but also took the corresponding rates of change into account ( $dT/dt$  and  $-dX/dt$ ). At the initial stage of drying, the viability of the bacteria was maintained at the initial level for a short period (Figure 6), which was a similar trend to the single droplet drying experiments. As drying progressed further, bacterial viability started to decrease. The drying process with 30 wt% skim milk as the protectant at 58 °C showed the earliest decrease in bacterial viability. Nevertheless, it gave the highest survival of  $37.31 \pm 21.90\%$  at the outlet of the drying tower (Figure 6c), which was very close to the experimental value ( $33.94 \pm 17.97\%$ ). Model 6 also accurately described the survival of *L. rhamnosus* GG in spray-dried powders when 10 and 20 wt% RSM were used as protectants at 58 °C, respectively ( $14.15 \pm 14.33\%$  and  $25.69 \pm 19.88\%$ , respectively; Figure 6a, b). At a higher temperature of 63 °C, the predicted survival by Model 6 at the spray dryer outlet ( $10.24 \pm 12.54\%$ ) was marginally lower than the experimental result ( $19.77 \pm 3.12\%$ ). Nevertheless, the prediction accuracy was still much better than that of the other five models, which substantially overestimated the residual viability of *L. rhamnosus* GG at the outlet (Figure 6d).

With Models 1–5, the degree of overestimation of bacterial survival varied with the form of the inactivation model (Figure 6). The viability curves calculated with Models 1 and 2 barely showed any downward trend throughout the drying process, with survivals higher than 98% at the outlet under all four drying conditions. Model 3 which considered the effect of  $T$

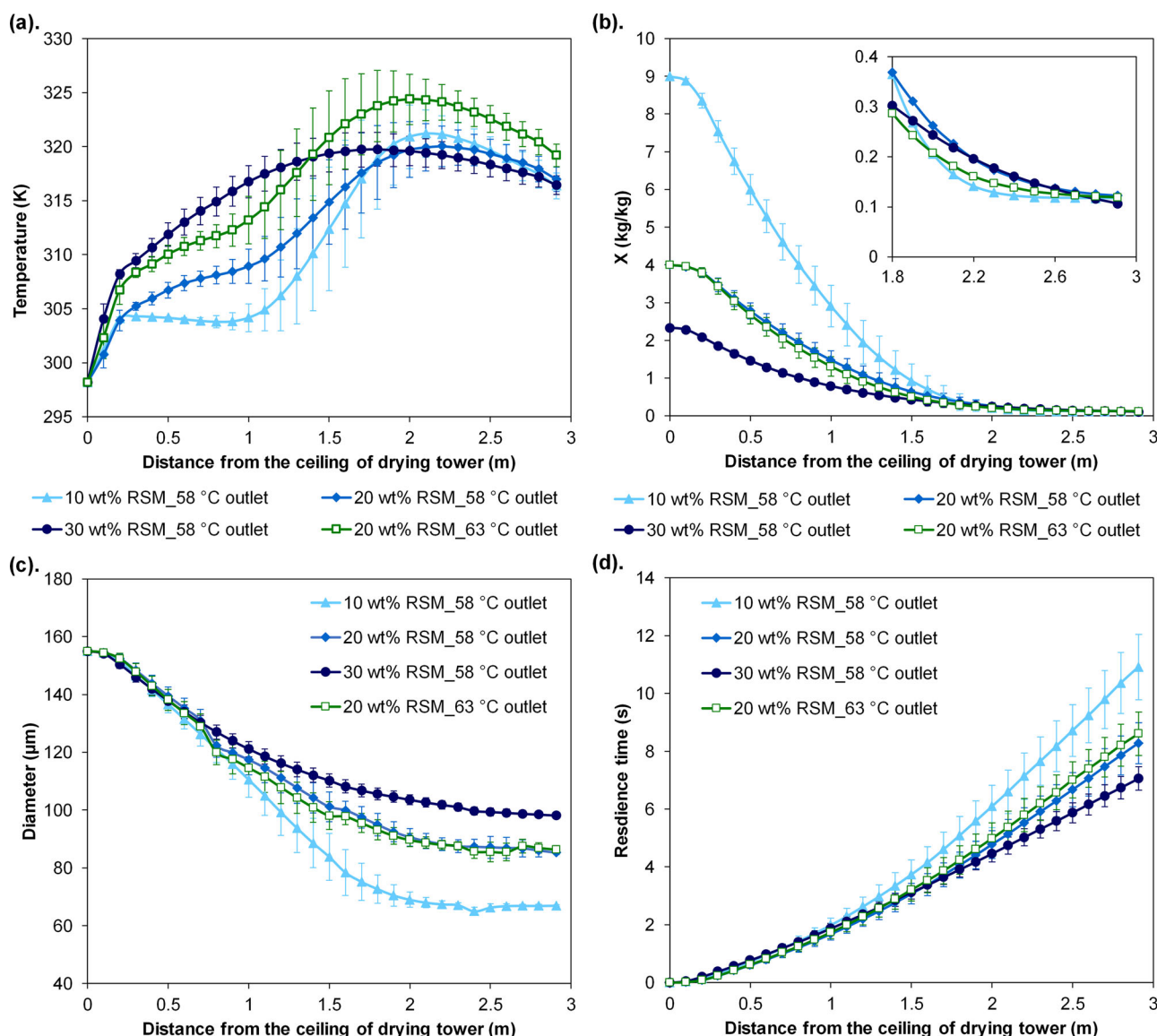


**Figure 4.** Changes in the physicochemical properties of *L. rhamnosus* GG-containing droplets along the axial direction of spray dryer, after flow field reached steady state in the CFD simulation. Error bars refer to the standard deviation of 2000 particles collected at the individual cross section. (a) Droplet temperature; (b) the moisture content of droplet; (c) droplet diameter; (d) residence time. For the outlet temperature of 58 °C, the protectant of 10, 20, and 30 wt% RSM was used, respectively. For the outlet temperature of 63 °C, the protectant was 20 wt% RSM.

and  $-dX/dt$  and Model 5 which considered the effect of  $T$ ,  $X$ , and  $dT/dt$  gave slightly higher deactivation; however, the residual viability remained greater than or equal to 95%. Involving  $T$ ,  $X$ , and  $-dX/dt$  as parameters, the viability curves predicted with Model 4 showed a descending trend from the middle section of the drying tower, with residual viability between 73% and 82% as affected by drying conditions. Models containing fewer drying kinetics parameters tend to have higher values of activation energy  $E_d$  (Table 5, Table S2, supplementary material), suggesting a relatively slow reaction rate and an increased difficulty for the inactivation reaction to occur. The trends in Figure 6 highlighted the importance of the

rates of change in accurately describing the inactivation of LAB cells during a rapid dehydration process such as spray drying.

The different capacity of the six models to describe the inactivation of *L. rhamnosus* GG during spray drying was double-checked using one-dimensional modeling, which assumed that the spray dryer was a 1-D plug-flow reactor.<sup>[38]</sup> Similar to the trends in Figure 6, only Model 6 accurately predicted the survival of *L. rhamnosus* GG at the outlet of the spray dryer, whereas the other five models all overestimated the residual viability of the bacteria (data not shown). For Models 2–5, the predicted survivals of spray-dried LGG calculated using 1-D modeling and using CFD



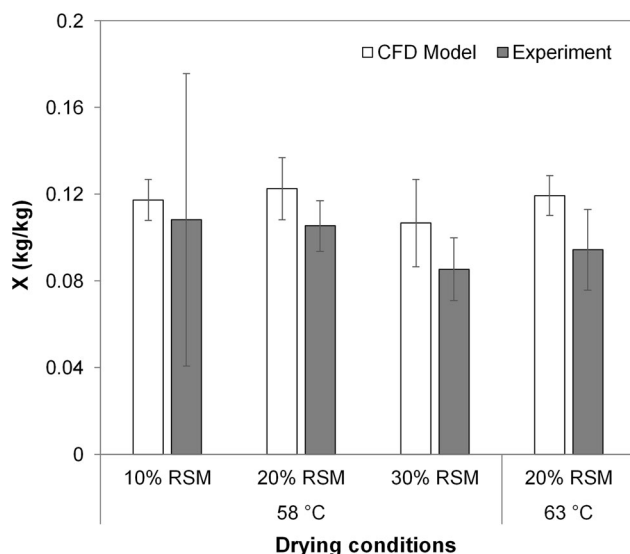


**Figure 5.** Comparison of the predicted moisture content of *L. rhamnosus* GG particles at the outlet of spray dryer to experimental results. Error bars of CFD data refer to the standard deviation of 2000 particles collected at the outlet plane. The temperatures of 58 and 63 °C referred to the outlet temperature of spray dryer.

showed differences between 3.5% and 25% at the outlet, while the viability curve predicted with Model 1 using 1-D modeling was maintained approximately at the initial value throughout the spray drying process. In the study of George et al.,<sup>[38]</sup> the 1-D modeling provided a reasonable description to the moisture content of skim milk particles produced using a microfluidic jet spray dryer. Perdana et al. modeled the inactivation processes of *Lactobacillus plantarum* WCFS1 in a pilot-scale spray dryer, assuming that the dryer was an ideal-mixed system and a plug flow system, respectively.<sup>[39]</sup> It was suggested that the actual drying profile should be between the two ideal cases.<sup>[39]</sup> In the present study, both CFD modeling and 1-D modeling demonstrated the better capacity of Model 6 in describing the inactivation of *L. rhamnosus* GG under wider dehydration conditions in comparison to Models 1–5.

Models 1–5 which were capable of describing the inactivation process of LAB during single droplet drying gave poor predictions about the survival of LAB after spray drying. The discrepancy might be linked to the difference in the rates of change between the two processes, which was up to 1–2 orders of magnitude. With 10 and 20 wt% RSM as the protectant, the time of drying during single droplet drying at 70 and 90 °C was between 200 and 400 s, giving averaged drying rates of 0.011–0.044 kg/kg/s. By contrast, the residence time of atomized droplets in spray drying ranged between 7 and 11 s (Figure 4d), with averaged drying

rates up to 0.31–0.81 kg/kg/s. The detrimental effects of the rates of change on LAB cells may be reasonably neglected in single droplet drying because of the low values, whereas in spray drying such effects could become critical, with such a high drying rate and the corresponding high rate of temperature change. The remarkable difference in both the time scale and the rates of change between single droplet drying and spray drying could be linked to the different initial sizes of the drying droplet (1.28–1.56 mm in single droplet drying and 155 µm in simulated spray drying).

Comparing the inactivation curves between Models 4, 5, and 6 in Figure 6, both  $dT/dt$  and  $-dX/dt$  appeared indispensable to the accurate description of LAB inactivation during spray drying, which could be related to the simultaneous heat- and mass-transfer nature of drying. Bacterial cells that contain complex cellular structures and a high intracellular water content could be sensitive to rapid changes in environmental conditions. Rapid dehydration may cause a large moisture content gradient across the cellular membrane, substantially increasing the level of osmotic stress exposure on cells.<sup>[18]</sup> Similarly, a large temperature gradient caused by rapid heating may also be detrimental to cellular integrity and biological functions.<sup>[40]</sup>

### Exploring the temporal and spatial changes for the inactivation of *L. rhamnosus* GG during spray drying

The dryer-wide simulation is capable of generating a large amount of data at intermediate drying stages, which are crucial to a better understanding of spray drying behavior and are difficult to monitor experimentally. First, the drying behavior before the injected droplets reached a steady state was studied. After a spray drying process was started, the initially injected droplets flew in the co-current hot airflow while the contained water was removed, reaching the bottom outlet of the dryer as dried particles in around 7–11 s (Figure 4d). The evaporation of water from the droplets lowered the temperature and increased the humidity of the flow field, which further impacted the evaporation behavior of subsequently injected droplets. To understand how the multiphase flow reached a steady state under different drying conditions, the temperature, moisture content, and survival profiles of atomized droplets at 10, 30, 60, 90, and 120 s after spray drying was started were compared in Figure 7. At the same outlet temperature of 58 °C, the three solid contents demonstrated distinct behaviors, despite the same initial droplet size of 155 µm and the



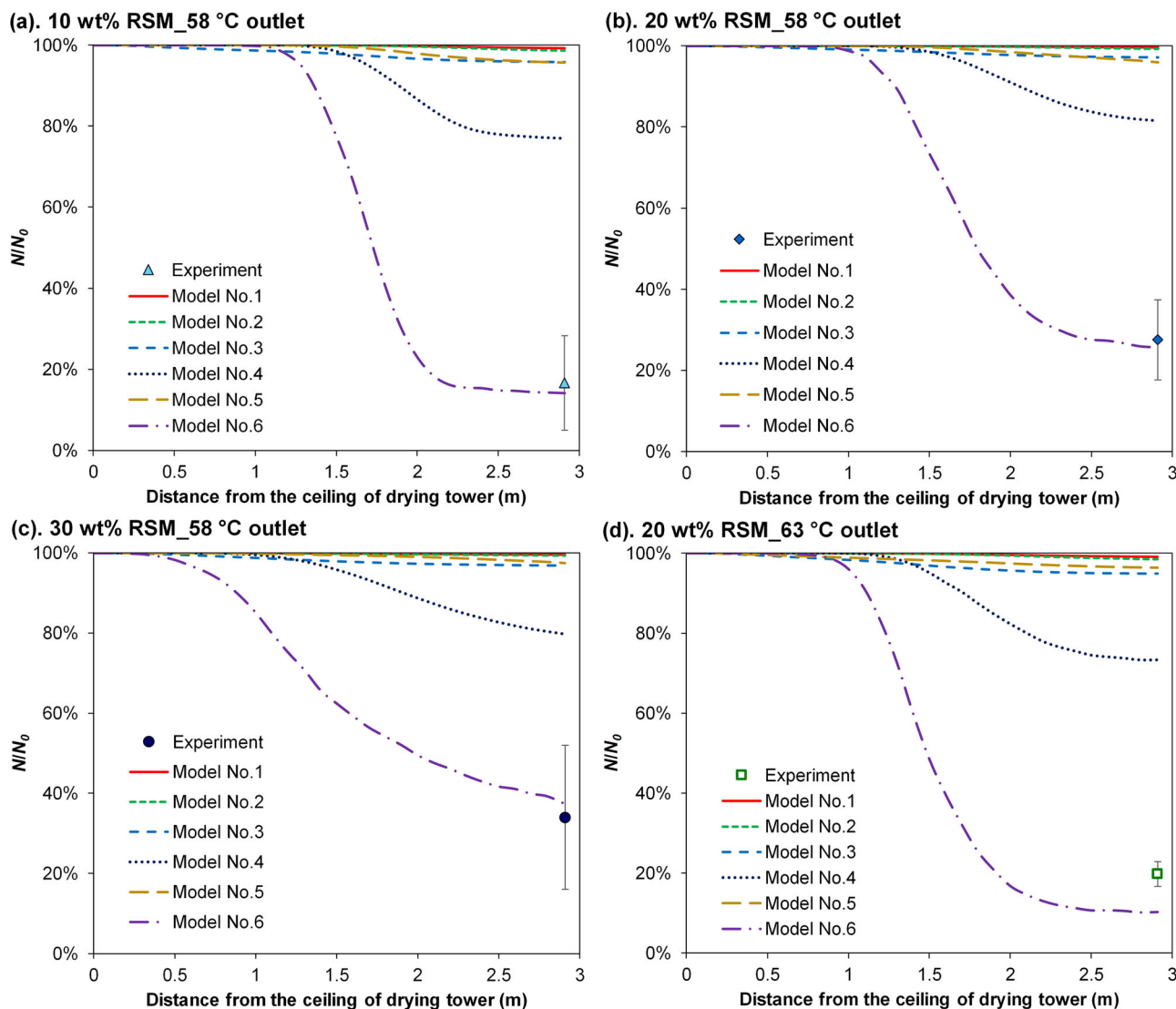


**Figure 6.** The inactivation process of *L. rhamnosus* GG along the axial direction of spray dryer in the CFD simulation, predicted by coupling Models 1–6 to the drying kinetics in Figure 4. (a) Using 10 wt% RSM as protectant at the outlet temperature of 58 °C; (b) using 20 wt% RSM as protectant at the outlet temperature of 58 °C; (c) using 30 wt% RSM as protectant at the outlet temperature of 58 °C; (d) using 20 wt% RSM as protectant at the outlet temperature of 63 °C.

same mass spray rate of  $2.2 \times 10^{-5} \text{ kg} \cdot \text{s}^{-1}$ . At 10 s after spray drying was started, the droplet temperature of 10 wt% RSM soared to 341 K following the web-bulb temperature range at around 305–308 K (Figure 7a). Heat transfer from the continuous gas phase to the evaporating droplets and the low temperature of injected droplets (298 K) lowered the temperature of the gas phase, which further led to a decrease of the peak temperature that the droplets could reach as spray drying was continued for a longer time. After spray drying was continued for 30 s, the droplet temperature curve was substantially lower than that of 10 s, with a difference larger than 15 K in peak temperature. The steady state was reached by 60 s of spray drying, as indicated by the overlapping temperature curves (Figure 7a). The difference in moisture content

curves became negligible at 30 s after spray drying was started (Figure 7b). The survival of *L. rhamnosus* GG at the outlet significantly increased from 0.06% at 10 s to 14.01% at 60 s, showing a difference of larger than two orders of magnitude (Figure 7c). The survival curve reached steady after 60 s rather than 30 s, indicating the dominating effect of droplet temperature on bacterial viability.

With the increase in the solid content of the protectant, atomized droplets took a longer time to reach the steady state in the continuous gas phase (Figure 7d–i). Since the flow field was kept identical for the three conditions before the injection of droplets, the difference may likely be linked to hindrance to mass transfer by the high solids. In the drying process with 30 wt% solids content, a minor difference was observed between the

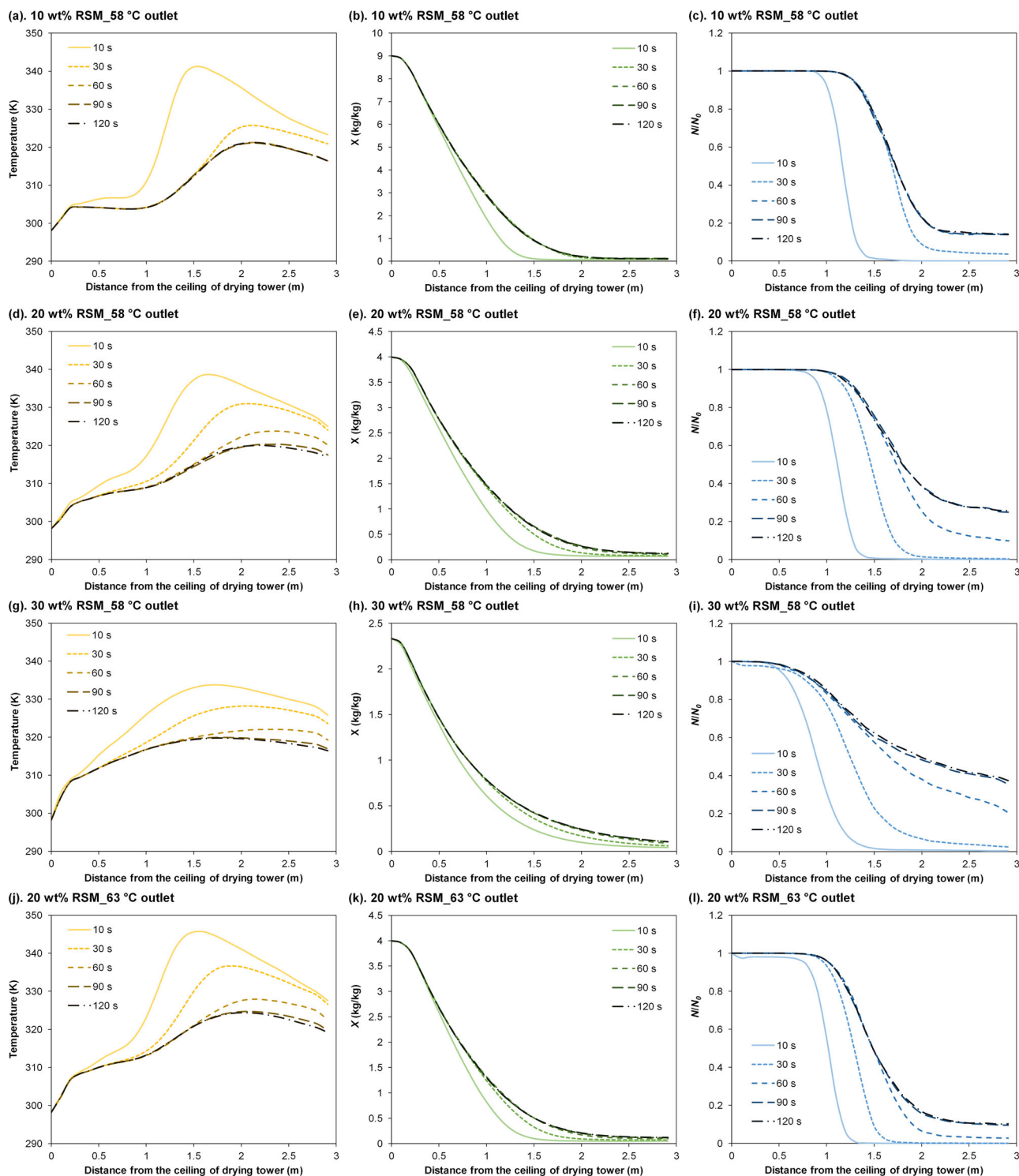


**Figure 7.** Changes in (a, d, g, j) the temperature of droplets, (b, e, h, k) the moisture content of droplets, and (c, f, i, l) the survival of *L. rhamnosus* GG along the axial direction of spray dryer, before the flow field reached steady state. (a–c) Using 10 wt% RSM as protectant at the outlet temperature of 58 °C; (d–f) using 20 wt% RSM as protectant at the outlet temperature of 58 °C; (g–i) using 30 wt% RSM as protectant at the outlet temperature of 58 °C; (j–l) using 20 wt% RSM as protectant at the outlet temperature of 63 °C.

survival curves after 90 and 120 s (Figure 7i). The use of a higher drying temperature of 63 °C accelerated water removal from atomized droplets and led to higher inactivation of *L. rhamnosus* GG than the drying process

at 58 °C (comparing Figure 7l and f). Nevertheless, with the same initial solids content of 20 wt%, the shift of the temperature and moisture content profiles in the initial 120 s of spray drying was similar for the drying

temperature of 63 and 58 °C (comparing Figure 7d–e and j–k).

LAB cells were found sensitive to drying kinetics in that a minor difference in drying kinetics could give rise to significant variations in the viability, membrane integrity, and digestive stability of dried bacteria; in the meantime, other particle properties such as particle morphology and rehydration behavior remained similar.<sup>[5]</sup> The sensitivity of LAB was supported by the varying survival curves in Figure 7c, f, i, and l, showing differences in viability for more than two orders of magnitude within the initial 2 min of spray drying. In the industrial production of common bio-active materials, a short unstable period at the beginning of spray drying is often negligible since the drying process often continues for hours. Nonetheless, the significantly lower viability of probiotics powder produced during the unstable period is disadvantageous to the quality of active probiotics products. It is probably better to separate the powders with low viability retention from those produced during the steady state period.

Next, the extent of the uniformity of LAB survival at the steady state was investigated (Figure 8 and 9). The simulated spray drying processes replicated the experimental processes of a microfluidic jet spray dryer, in which monodisperse droplets were dehydrated in optimized air dynamics to produce particles with identical size, morphology, and properties.<sup>[25,41]</sup> From the simulation, the flying droplets demonstrated noticeable variations in the survival of *L. rhamnosus* GG in the middle section of the spray dryer (Figure 8). As the droplets flew toward the bottom outlet, the decrease in the viability of *L. rhamnosus* GG was first observed for droplets close to the wall of the dryer. Droplets at the center region maintained high viability till a later drying stage, as indicated by the gradually diminishing red and orange dots along the axial direction of the spray dryer (Figure 8a–d). The trend was in correspondence with the lower droplet temperature and higher moisture content shown by the droplets at the center region when they reached the middle section of the dryer (Figure 9). The relatively uneven distribution of droplet properties and *L. rhamnosus* GG survival in the cross-section may likely be linked to the degree of crowding of droplets. After injection, the stream of droplets quickly dispersed to achieve a more efficient mixing with the co-current airflow. Nevertheless, the center region concentrated a higher number of droplets, as can be seen from the bottom view of the simulated spray dryer (Figures 8 and 9). Such a flow pattern of droplets may help reduce wall

deposition and thus improve the yield of spray-dried particles. As droplets approached the outlet, the difference in droplet properties became minimal, as reflected by error bars in Figure 4a–c. In future studies, further improvement in the similarity of the drying histories of atomized droplets may be achieved by optimizing the mixing behavior of droplets and hot air.

Compared to the curves in Figure 4a and b, the dot plots in Figure 9 provided additional information on the drying behavior of atomized droplets. The three moisture content curves of 10, 20, and 30 wt% RSM at 58 °C in Figure 4b showed substantial differences because of the different initial moisture contents. Nevertheless, when changes in moisture content were normalized to the same color scale, the trends of the decrease in particle moisture content were relatively similar between the three drying processes (Figure 9e–g).

A significant decrease in the viability of *L. rhamnosus* GG was observed at the bottom half of the drying tower when 10 wt% RSM was used as the protectant at 58 °C, as indicated by the large number of dark blue dots in Figure 8a. The extent of inactivation was lessened with 20 wt% RSM (Figure 8b). The drying process of 30 wt% RSM showed a remarkably lower degree of inactivation than that with 10 and 20 wt% RSM (Figure 8c). The trend was in agreement with the report of Ghandi et al.,<sup>[42]</sup> which showed that the protective effect of a composite protectant increased as solid content was increased from 10, 25, to 35 wt% in the spray drying of *L. cremoris*. These results indicated that the relatively mild kinetics of temperature change and moisture content change given by a protectant of a high solid content is advantageous to the preservation of bacterial viability through spray drying.

Previous studies attempted to model the inactivation of spray-dried LAB cells using various approaches. Empirical modeling, such as response surface methodology, has been used to correlate the survival of LAB to the operation conditions of the specific spray dryer.<sup>[43,44]</sup> For describing changes in the viability of LAB inside a spray dryer, Perdana et al. utilized a modeling software pack entitled DryProf to model droplet drying kinetics based on the effective diffusion concept.<sup>[45]</sup> The retention of the viability of LAB was calculated using the Weibull model. Optimal spray drying conditions with LAB residual viability larger than 80% were recommended as small initial droplet size, hollow particle morphology, low outlet temperature, and an ideal-mixed dryer system.<sup>[45]</sup> Menshutina et al. combined mass, momentum, and energy conservation equations for the gaseous and dispersed phases to model a spray drying process, and the loss of the viability of *Bifidobacterium*

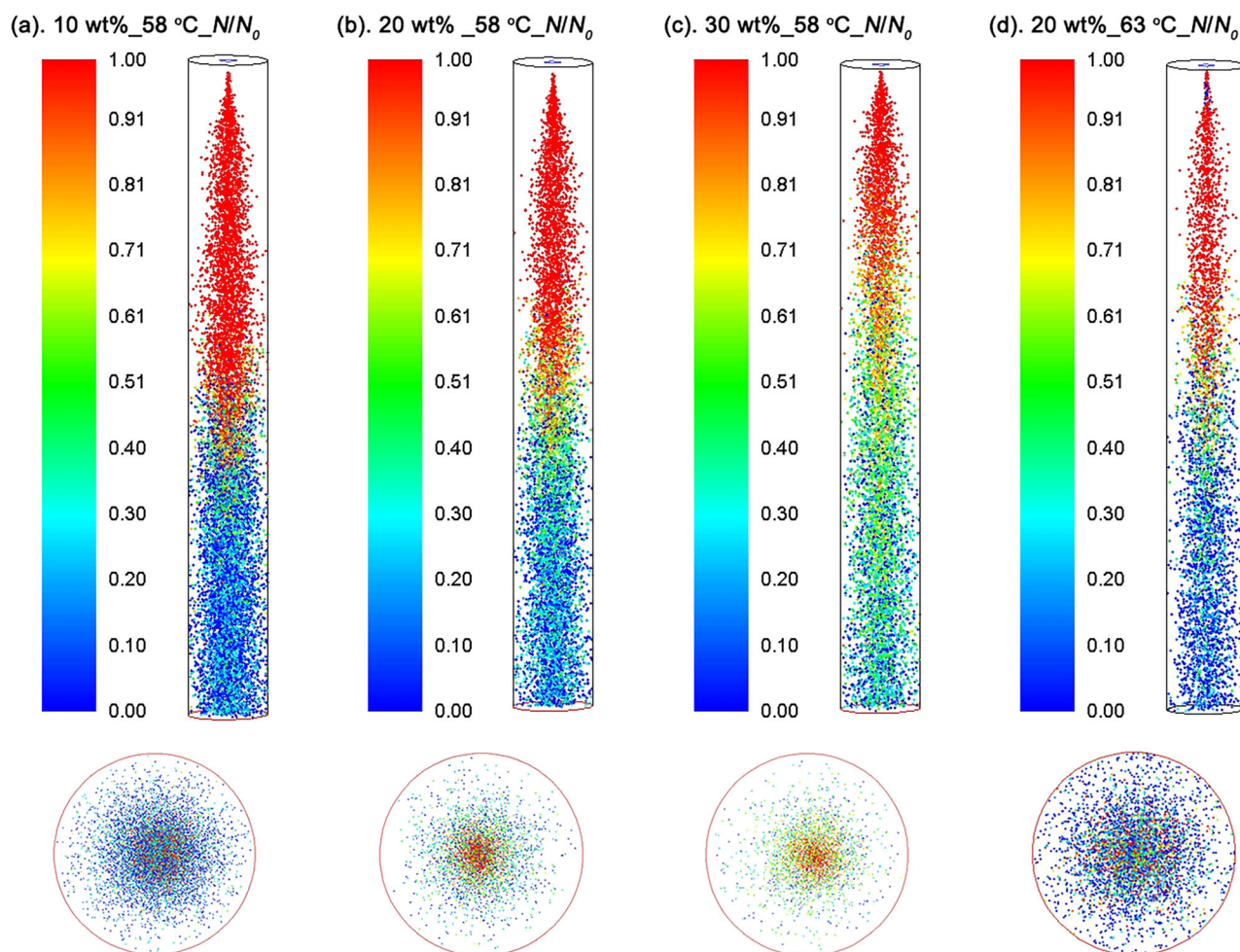


**Figure 8.** The spatial distribution of the survival of *L. rhamnosus* GG at the steady state from the front view and bottom view. (a) Using 10 wt% RSM as protectant at the outlet temperature of 58 °C; (b) using 20 wt% RSM as protectant at the outlet temperature of 58 °C; (c) using 30 wt% RSM as protectant at the outlet temperature of 58 °C; (d) using 20 wt% RSM as protectant at the outlet temperature of 63 °C.

*bifidum* caused by thermal stress was described using the standard Arrhenius equation as shown in Equation (2).<sup>[46]</sup> The present study demonstrated that the incorporation of the rates of temperature and moisture content change in the inactivation model allows the model to be used under wider drying conditions, including both slow and rapid droplet drying. In addition, CFD simulation enabled investigations on the variation of LAB viability with the time of spray drying and the distribution of LAB viability inside the spray dryer.

## Conclusions

This study proposed a model that can accurately describe the inactivation process of *L. rhamnosus* GG, a model LAB strain, during both single droplet drying and spray drying. The inactivation profile of *L. rhamnosus* GG inside a spray dryer was monitored, by coupling the proposed inactivation model to the drying kinetics

of a microfluidic jet spray dryer on the ANSYS FLUENT platform. A total of six inactivation models were tested, all in the form of Arrhenius-type equations but considering different combinations of drying kinetics parameters, namely, droplet temperature ( $T$ ), moisture content ( $X$ ), the rate of temperature change ( $dT/dt$ ), and drying rate ( $-dX/dt$ ). All six models well described the inactivation process of *L. rhamnosus* GG during single droplet drying, a comparatively slow drying process analogous to spray drying. By contrast, only Model 6 which incorporated all four parameters accurately predicted the survival of *L. rhamnosus* GG in spray-dried particles. The results highlighted the importance of the rates of temperature and moisture content change on the viability of LAB cells in the rapidly changing droplet environment during spray drying, with average drying rates of 0.31–0.81 kg/kg/s. The successful modeling of the inactivation process of LAB allowed the quantitative analysis of the temporal and



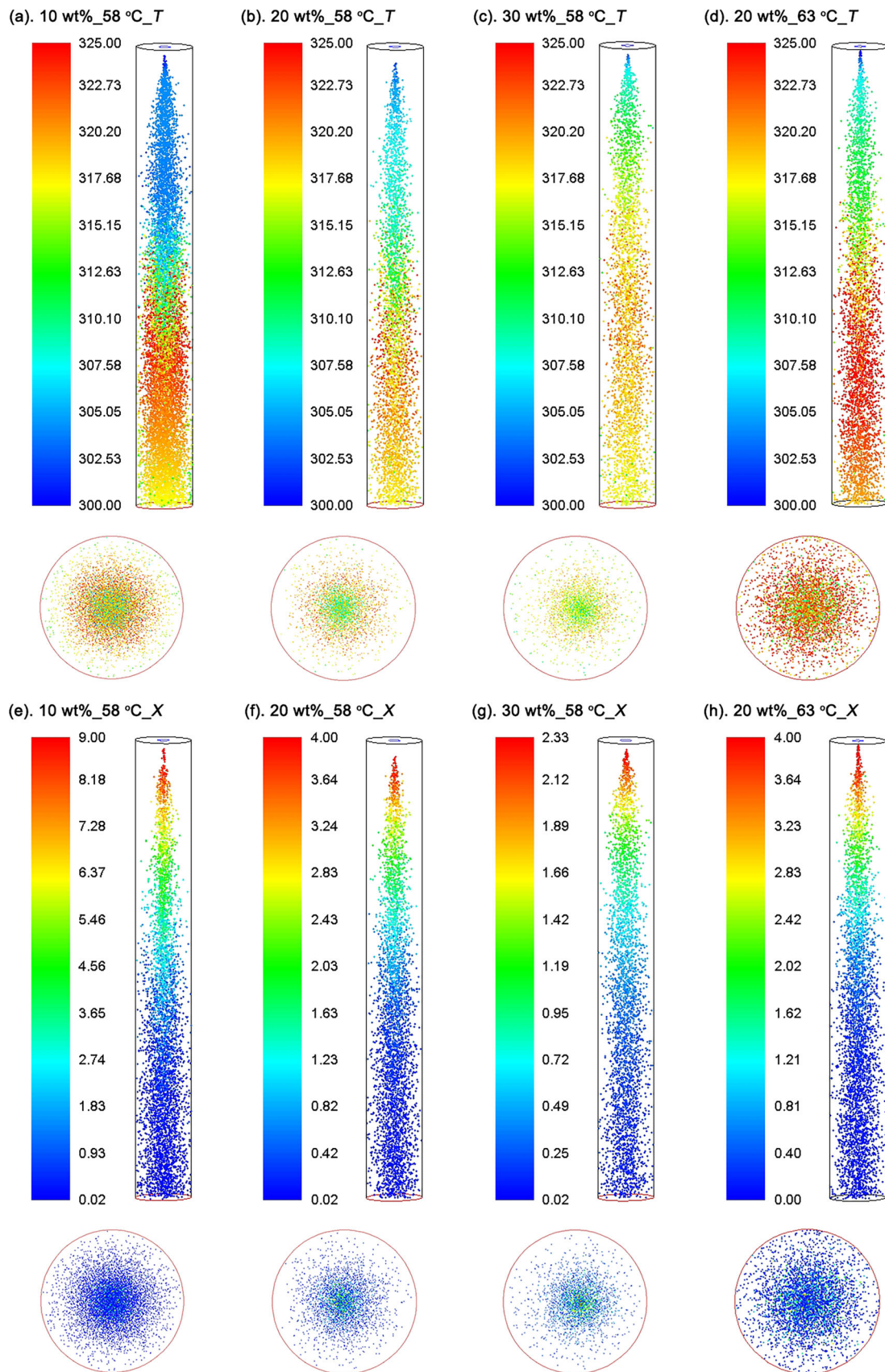


**Figure 9.** The spatial distribution of (a–d) the temperature of droplets and (e–h) the moisture content of droplets at the steady state from the front view and bottom view. (a, e) Using 10 wt% RSM as protectant at the outlet temperature of 58 °C; (b, f) using 20 wt% RSM as protectant at the outlet temperature of 58 °C; (c, g) using 30 wt% RSM as protectant at the outlet temperature of 58 °C; (d, h) using 20 wt% RSM as protectant at the outlet temperature of 63 °C.



spatial changes of LAB viability during spray drying. The proposed inactivation model is potential to be applied in other types of spray dryers through coupling with the drying kinetics of the specific dryer. Since the model was developed with a limited number of single droplet drying experiments, future studies may work on the optimization of the model to further improve the accuracy of prediction.

## Nomenclature

### Letters

$\Delta E_v$	The apparent activation energy of evaporation (J/mol)
$\Delta H_l$	The specific enthalpy of water evaporation (J/kg)
$A$	Surface area ( $\text{m}^2$ )
$C$	A given quality attribute of food material, herein the survival of lactic acid bacteria ( $N/N_0$ )
$C_d$	Drag coefficient
$c_p$	Specific heat capacity at constant pressure (J/(kg·K))
$D$	Diameter (m)
$E_d$	The activation energy needed for the inactivation of bacteria (J/mol)
$h$	heat transfer coefficient ( $\text{W}/(\text{m}^2 \cdot \text{K})$ )
$h_m$	mass transfer coefficient (m/s)
$k$	Inactivation rate of bacteria
$k_0$	Pre-exponential factor
$m$	Mass (kg)
$N$	The viable cell count of bacteria (cfu/mL)
$Re$	Reynolds number
$t$	Time (s)
$T$	Temperature (K)
$u$	Velocity (m/s)
$X$	Moisture content on a dry basis (kg/kg)

### Greek letters

$\rho$	Density ( $\text{kg}/\text{m}^3$ )
$\psi$	Fractionality coefficient in the REA model

### Subscripts

0	The initial state
b	Bulk gas
d	Deactivation
e	Equilibrium
p	Particle
s	Solids
sur	Surface
sat	Saturation
v	Vapor or vaporization

### Abbreviations

LAB	Lactic acid bacteria
LGG	<i>Lactobacillus rhamnosus</i> GG, <i>L. rhamnosus</i> GG

REA model	Reaction Engineering Approach model
RSM	Reconstituted skim milk

## Disclosure statement

The authors report no conflicts of interest. The authors alone are responsible for the content and writing of the paper.

## Funding

This work was supported by the Natural Science Foundation of China [grant numbers 22178239, 21978184], Jiangsu Agriculture Science and Technology Innovation Fund (JASTIF, grant number CX(20)3048), and the Priority Academic Program Development (PAPD) of Jiangsu Higher Education Institutions.

## References

- [1] Xu, Y. N.; Zeng, L. P.; Xiao, N.; Wang, C.; Liang, Z. H.; Wu, Q. J.; Zhang, Y. J.; Du, B.; Li, P. Quality Enhancement of Dendrobium Officinale and Banana Juice through Probiotic Fermentation Using Beneficial Lactic Acid-Producing Bacteria. *Int. J. Food Eng.* **2020**, *16*, 20190370. DOI: [10.1515/ijfe-2019-0370](https://doi.org/10.1515/ijfe-2019-0370).
- [2] Wang, N.; Fu, N.; Chen, X. D. The Extent and Mechanism of the Effect of Protectant Material in the Production of Active Lactic Acid Bacteria Powder Using Spray Drying: A Review. *Curr. Opin. Food Sci.* **2022**, *44*, 100807. DOI: [10.1016/j.cofs.2022.01.003](https://doi.org/10.1016/j.cofs.2022.01.003).
- [3] Di Battista, C. A.; Constenla, D.; Rigo, M. V. R.; Piña, J. Process Analysis and Global Optimization for the Microencapsulation of Phytosterols by Spray Drying. *Powder Technol.* **2017**, *321*, 55–65. DOI: [10.1016/j.powtec.2017.08.008](https://doi.org/10.1016/j.powtec.2017.08.008).
- [4] Perdana, J.; Bereschenko, L.; Fox, M. B.; Kuperus, J. H.; Kleerebezem, M.; Boom, R. M.; Schutyser, M. A. I. Dehydration and Thermal Inactivation of *Lactobacillus plantarum* WCFS1: Comparing Single Droplet Drying to Spray and Freeze Drying. *Food Res. Int.* **2013**, *54*, 1351–1359. DOI: [10.1016/j.foodres.2013.09.043](https://doi.org/10.1016/j.foodres.2013.09.043).
- [5] Mao, H.; Chen, X. D.; Fu, N. Exploring the Integrity of Cellular Membrane and Resistance to Digestive Juices of Dehydrated Lactic Acid Bacteria as Influenced by Drying Kinetics. *Food Res. Int.* **2022**, *157*, 111395. DOI: [10.1016/j.foodres.2022.111395](https://doi.org/10.1016/j.foodres.2022.111395).
- [6] Liu, H.; Gong, J.; Chabot, D.; Miller, S. S.; Cui, S. W.; Zhong, F.; Wang, Q. Improved Survival of *Lactobacillus zeae* LB1 in a Spray Dried Alginate-Protein Matrix. *Food. Hydrocolloids.* **2018**, *78*, 100–108. DOI: [10.1016/j.foodhyd.2017.07.004](https://doi.org/10.1016/j.foodhyd.2017.07.004).
- [7] Jiang, N.; Dev Kumar, G.; Chen, J.; Mishra, A.; Mis Solval, K. Comparison of Concurrent and Mixed-Flow Spray Drying on Viability, Growth Kinetics and Biofilm Formation of *Lactobacillus rhamnosus* GG Microencapsulated with Fish Gelatin and Maltodextrin. *LWT – Food Sci. Technol.* **2020**, *124*, 109200. DOI: [10.1016/j.lwt.2020.109200](https://doi.org/10.1016/j.lwt.2020.109200).

- [8] Hao, F.; Fu, N.; Ndiaye, H.; Woo, M. W.; Jeantet, R.; Chen, X. D. Thermotolerance, Survival, and Stability of Lactic Acid Bacteria after Spray Drying as Affected by the Increase of Growth Temperature. *Food. Bioprocess Technol.* **2021**, *14*, 120–132. DOI: [10.1007/s11947-020-02571-1](https://doi.org/10.1007/s11947-020-02571-1).
- [9] Woo, M. W.; Daud, W. R. W.; Mujumdar, A. S.; Talib, M. Z. M.; Hua, W. Z.; Masrinda, T. S. Comparative Study of Droplet Drying Models for CFD Modelling. *Chem. Eng. Res. Des.* **2008**, *86*, 1038–1048. DOI: [10.1016/j.cherd.2008.04.003](https://doi.org/10.1016/j.cherd.2008.04.003).
- [10] Fu, N.; Woo, M. W.; Selomulya, C.; Chen, X. D. Inactivation of *Lactococcus lactis* Ssp. *cremoris* Cells in a Droplet during Convective Drying. *Biochem. Eng. J.* **2013**, *79*, 46–56. DOI: [10.1016/j.bej.2013.06.015](https://doi.org/10.1016/j.bej.2013.06.015).
- [11] Perdana, J.; Fox, M. B.; Siwei, C.; Boom, R. M.; Schutyser, M. A. I. Interactions between Formulation and Spray Drying Conditions Related to Survival of *Lactobacillus plantarum* WCFS1. *Food Res. Int.* **2014**, *56*, 9–17. DOI: [10.1016/j.foodres.2013.12.007](https://doi.org/10.1016/j.foodres.2013.12.007).
- [12] Ghandi, A.; Powell, I.; Chen, X. D.; Adhikari, B. Drying Kinetics and Survival Studies of Dairy Fermentation Bacteria in Convective Air Drying Environment Using Single Droplet Drying. *J. Food Eng.* **2012**, *110*, 405–417. DOI: [10.1016/j.jfoodeng.2011.12.031](https://doi.org/10.1016/j.jfoodeng.2011.12.031).
- [13] Xiao, J.; Yang, S.; George, O. A.; Putranto, A.; Wu, W. D.; Chen, X. D. Numerical Simulation of Mono-Disperse Droplet Spray Dryer: Coupling Distinctively Different Sized Chambers. *Chem. Eng. Sci.* **2019**, *200*, 12–26. DOI: [10.1016/j.ces.2019.01.030](https://doi.org/10.1016/j.ces.2019.01.030).
- [14] Maryamnegari, S. M.; Ashrafizadeh, A.; Baake, E.; Guglielmi, M. Effects of Thermal Boundary Conditions on the Performance of Spray Dryers. *J. Food Eng.* **2023**, *338*, 111250. DOI: [10.1016/j.jfoodeng.2022.111250](https://doi.org/10.1016/j.jfoodeng.2022.111250).
- [15] Jubaer, H.; Afshar, S.; Xiao, J.; Chen, X. D.; Selomulya, C.; Woo, M. W. On the Importance of Droplet Shrinkage in CFD-Modeling of Spray Drying. *Drying Technol.* **2018**, *36*, 1785–1801. DOI: [10.1080/07373937.2017.1349791](https://doi.org/10.1080/07373937.2017.1349791).
- [16] Jaskulski, M.; Tran, T. T. H.; Tsotsas, E. Design Study of Printer Nozzle Spray Dryer by Computational Fluid Dynamics Modeling. *Drying Technol.* **2020**, *38*, 211–223. DOI: [10.1080/07373937.2019.1633541](https://doi.org/10.1080/07373937.2019.1633541).
- [17] Heldman, D. R.; Hartel, R. W. Chapter 1. Introduction. In *Principles of Food Processing*; Heldman, D.R.; Hartel, R.W., Eds.; Aspen Publishers: New York, **1997**; pp. 1–12.
- [18] Marechal, P. A.; Martínez de Marnañón, I.; Poirier, I.; Gervais, P. The Importance of the Kinetics of Application of Physical Stresses on the Viability of Microorganisms: Significance for Minimal Food Processing. *Trends Food Sci. Techn.* **1999**, *10*, 15–20. DOI: [10.1016/S0924-2244\(99\)00012-6](https://doi.org/10.1016/S0924-2244(99)00012-6).
- [19] Poirier, I.; Marechal, P.-A.; Gervais, P. Effects of the Kinetics of Water Potential Variation on Bacteria Viability. *J. Appl. Microbiol.* **1997**, *82*, 101–106. DOI: [10.1111/j.1365-2672.1997.tb03303.x](https://doi.org/10.1111/j.1365-2672.1997.tb03303.x).
- [20] Gong, P.; Sun, J.; Lin, K.; Di, W.; Zhang, L.; Han, X. Changes Process in the Cellular Structures and Constituents of *Lactobacillus bulgaricus* sp1.1 during Spray Drying. *LWT – Food Sci. Technol.* **2019**, *102*, 30–36. DOI: [10.1016/j.lwt.2018.12.005](https://doi.org/10.1016/j.lwt.2018.12.005).
- [21] Hlaing, M. M.; Wood, B. R.; McNaughton, D.; Ying, D.; Dumsday, G.; Augustin, M. A. Effect of Drying Methods on Protein and DNA Conformation Changes in *Lactobacillus rhamnosus* GG Cells by Fourier Transform Infrared Spectroscopy. *J. Agric. Food Chem.* **2017**, *65*, 1724–1731. DOI: [10.1021/acs.jafc.6b05508](https://doi.org/10.1021/acs.jafc.6b05508).
- [22] Chen, X. D.; Patel, K. C. Micro-Organism Inactivation during Drying of Small Droplets or Thin-Layer slabs - A Critical Review of Existing Kinetics Models and an Appraisal of the Drying Rate Dependent Model. *J. Food Eng.* **2007**, *82*, 1–10. DOI: [10.1016/j.jfoodeng.2006.12.013](https://doi.org/10.1016/j.jfoodeng.2006.12.013).
- [23] Huang, H.; Brooks, M. S. L.; Huang, H. J.; Chen, X. D. Inactivation Kinetics of Yeast Cells during Infrared Drying. *Drying Technol.* **2009**, *27*, 1060–1068. DOI: [10.1080/07373930903218453](https://doi.org/10.1080/07373930903218453).
- [24] Zheng, X.; Fu, N.; Duan, M.; Woo, M. W.; Selomulya, C.; Chen, X. D. The Mechanisms of the Protective Effects of Reconstituted Skim Milk during Convective Droplet Drying of Lactic Acid Bacteria. *Food. Res. Int.* **2015**, *76*, 478–488. DOI: [10.1016/j.foodres.2015.07.045](https://doi.org/10.1016/j.foodres.2015.07.045).
- [25] Wu, W. D.; Amelia, R.; Hao, N.; Selomulya, C.; Zhao, D.; Chiu, Y.-L.; Chen, X. D. Assembly of Uniform Photoluminescent Microcomposites Using a Novel Micro-Fluidic-Jet-Spray-Dryer. *AIChE J.* **2011**, *57*, 2726–2737. DOI: [10.1002/aic.12489](https://doi.org/10.1002/aic.12489).
- [26] Su, Y.; Zheng, X.; Zhao, Q.; Fu, N.; Xiong, H.; Wu, W. D.; Chen, X. D. Spray Drying of *Lactobacillus rhamnosus* GG with Calcium-Containing Protectant for Enhanced Viability. *Powder Technol.* **2019**, *358*, 87–94. DOI: [10.1016/j.powtec.2018.09.082](https://doi.org/10.1016/j.powtec.2018.09.082).
- [27] Zastawny, M.; Mallouppas, G.; Zhao, F.; Van Wachem, B. Derivation of Drag and Lift Force and Torque Coefficients for Non-Spherical Particles in Flows. *Int. J. Multiphase Flow.* **2012**, *39*, 227–239. DOI: [10.1016/j.ijmultiphaseflow.2011.09.004](https://doi.org/10.1016/j.ijmultiphaseflow.2011.09.004).
- [28] Clift, R.; Grace, J. R.; Weber, M. E. *Bubbles, Drops and Particles*, 1st ed.; Academic Press, Inc.: New York, USA, **1978**; p. 380.
- [29] Lin, S.; Chen, X. D. Changes in Milk Droplet Diameter during Drying under Constant Drying Conditions Investigated Using the Glass-Filament Method. *Food Bioprod. Process.* **2004**, *82*, 213–218. DOI: [10.1205/fbio.82.3.213.44178](https://doi.org/10.1205/fbio.82.3.213.44178).
- [30] Chen, X. D.; Lin, S. X. Q. Air Drying of Milk Droplet under Constant and Time-Dependent Conditions. *AIChE J.* **2005**, *51*, 1790–1799. DOI: [10.1002/aic.10449](https://doi.org/10.1002/aic.10449).
- [31] Delignette-Muller, M. L. Principles of Predictive Modeling. In *Safety of Meat and Processed Meat*; Toldra, F., Ed. New York: Springer Science + Business Media, LLC., **2009**; pp. 535–557. DOI: [10.1007/978-0-387-89026-5\\_21](https://doi.org/10.1007/978-0-387-89026-5_21).
- [32] Peleg, M.; Cole, M. B. Reinterpretation of Microbial Survival Curves. *Crit. Rev. Food Sci. Nutr.* **1998**, *38*, 353–380. DOI: [10.1080/10408699891274246](https://doi.org/10.1080/10408699891274246).
- [33] Mendes-Oliveira, G.; Jensen, J. L.; Keener, K. M.; Campanella, O. H. Modeling the Inactivation of

- Bacillus subtilis* Spores during Cold Plasma Sterilization. *Innov. Food Sci. Emerg. Technol.* **2019**, 52, 334–342. DOI: [10.1016/j.ifset.2018.12.011](https://doi.org/10.1016/j.ifset.2018.12.011).
- [34] Yoon, J.-H.; Han, A.; Paek, J.; Lee, S.-Y. Evaluation of Non-Isothermal Inactivation on Survivals of Pathogenic Bacteria by Predictive Models. *LWT – Food Sci. Technol.* **2019**, 101, 366–373. DOI: [10.1016/j.lwt.2018.11.023](https://doi.org/10.1016/j.lwt.2018.11.023).
- [35] Peleg, M. Calculation of the Non-Isothermal Inactivation Patterns of Microbes Having Sigmoidal Isothermal Semi-Logarithmic Survival Curves. *Crit. Rev. Food Sci. Nutr.* **2003**, 43, 645–658. DOI: [10.1080/10408690390251156](https://doi.org/10.1080/10408690390251156).
- [36] Zhou, X.; Dong, J.; Gao, J.; Yu, Z. Activity-Loss Characteristics of Spores of *Bacillus thuringiensis* during Spray Drying. *Food Bioprod. Pro.* **2008**, 86, 37–42. DOI: [10.1016/j.fbp.2007.10.017](https://doi.org/10.1016/j.fbp.2007.10.017).
- [37] Rogers, S.; Wu, W. D.; Lin, S. X. Q.; Chen, X. D. Particle Shrinkage and Morphology of Milk Powder Made with a Monodisperse Spray Dryer. *Biochem. Eng. J.* **2012**, 62, 92–100. DOI: [10.1016/j.bej.2011.11.002](https://doi.org/10.1016/j.bej.2011.11.002).
- [38] George, O. A.; Chen, X. D.; Xiao, J.; Woo, M.; Che, L. An Effective Rate Approach to Modeling Single-Stage Spray Drying. *AIChE J.* **2015**, 61, 4140–4151. DOI: [10.1002/aic.14940](https://doi.org/10.1002/aic.14940).
- [39] Perdana, J.; Aguirre Zubia, A.; Kutahya, O.; Schutyser, M.; Fox, M. Spray Drying of *Lactobacillus plantarum* WCFS1 Guided by Predictive Modeling. *Drying Technol.* **2015**, 33, 1789–1797. DOI: [10.1080/07373937.2015.1026975](https://doi.org/10.1080/07373937.2015.1026975).
- [40] Gervais, P.; Martinez de Marañon, I. Effect of the Kinetics of Temperature Variation on *Saccharomyces cerevisiae* Viability and Permeability. *Biochim. Biophys. Acta.* **1995**, 1235, 52–56. DOI: [10.1016/0005-2736\(94\)00299-5](https://doi.org/10.1016/0005-2736(94)00299-5).
- [41] Xiong, X.; Zhang, S.; Fu, N.; Lei, H.; Wu, W. D.; Chen, X. D. Effects of Particle Formation Behavior on the Properties of Fish Oil Microcapsules Fabricated Using a Micro-Fluidic Jet Spray Dryer. *Int. J. Food Eng.* **2021**, 17, 27–36. DOI: [10.1515/ijfe-2019-0162](https://doi.org/10.1515/ijfe-2019-0162).
- [42] Ghandi, A.; Powell, I. B.; Chen, X. D.; Adhikari, B. The Effect of Dryer Inlet and Outlet Air Temperatures and Protectant Solids on the Survival of *Lactococcus lactis* during Spray Drying. *Drying Technol.* **2012**, 30, 1649–1657. DOI: [10.1080/07373937.2012.703743](https://doi.org/10.1080/07373937.2012.703743).
- [43] Anekella, K.; Orsat, V. Optimization of Microencapsulation of Probiotics in Raspberry Juice by Spray Drying. *LWT – Food Sci. Technol.* **2013**, 50, 17–24. DOI: [10.1016/j.lwt.2012.08.003](https://doi.org/10.1016/j.lwt.2012.08.003).
- [44] Ahlawat, A.; Basak, S.; Ananthanarayan, L. Optimization of Spray-Dried Probiotic Buttermilk Powder Using Response Surface Methodology and Evaluation of Its Shelf Stability. *Food Process. Preserv.* **2022**, 46, e16928. DOI: [10.1111/jfpp.16928](https://doi.org/10.1111/jfpp.16928).
- [45] Perdana, J.; Fox, M. B.; Boom, R. M.; Schutyser, M. A. I. Establishing Guidelines to Retain Viability of Probiotics during Spray Drying. *Drying Technol.* **2015**, 33, 1560–1569. DOI: [10.1080/07373937.2015.1012264](https://doi.org/10.1080/07373937.2015.1012264).
- [46] Menshutina, N. V.; Gordienko, M. G.; Voinovskiy, A. A.; Zbicinski, I. Spray Drying of Probiotics: Process Development and Scale-Up. *Drying Technol.* **2010**, 28, 1170–1177. DOI: [10.1080/07373937.2010.483043](https://doi.org/10.1080/07373937.2010.483043).